SUPPORTING INFORMATION FOR:

Understanding the electronic factors responsible for ligand spin-orbit NMR shielding in transition-metal complexes

Jan Vícha,[†] Cina Foroutan-Nejad,[†,‡] Tomasz Pawlak,[†,Δ] Markéta L. Munzarová,[†,$] Michal Straka,[†,ǁ,*] and Radek Marek[†,$,*]

[†] *CEITEC - Central European Institute of Technology, Masaryk University, Kamenice 5/A4, CZ-62500 Brno, Czech Republic*

[‡] *National Centre for Biomolecular Research, Faculty of Science, Masaryk University, Kamenice 5, CZ-62500 Brno, Czech Republic*

[$] *Department of Chemistry, Faculty of Science, Masaryk University, Kamenice 5, CZ-62500 Brno, Czech Republic*

[ǁ] *Institute of Organic Chemistry and Biochemistry of the ASCR, Flemingovo nám. 2, CZ-16610, Praha , Czech Republic*

METHODS

Quantum Theory of Atoms in Molecules

The geometries of **19-21** optimized at PBE0/def2-TZVPP level were used for QTAIM analysis. Auxiliary *s*-type core electron functions were added manually to the molecular wave functions to model the ECP core electrons of I atom (for details, see the article).

SOS-DFTP, Equation S1

$$\sigma_{vu}^{p} = \frac{i}{\lambda_N}\left[\frac{e\hbar}{2mc} B_v \sum_k^{occ\,\alpha} \sum_a^{virt\,\alpha} \frac{\langle\varphi_k^{\alpha}(\lambda_N)|\hat{\mathbf{l}}_v|\varphi_a^{\alpha}(\lambda_N)\rangle\langle\varphi_a^{\alpha}(\lambda_N)|\widehat{\mathbf{H}}_u^{\mathbf{SO}}|\varphi_k^{\alpha}(\lambda_N)\rangle}{\varepsilon_k - \varepsilon_a}\right] - \frac{i}{\lambda_N}\left[\frac{e\hbar}{2mc} B_v \sum_k^{occ\,\beta} \sum_a^{virt\,\beta} \frac{\langle\varphi_k^{\beta}(\lambda_N)|\hat{\mathbf{l}}_v|\varphi_a^{\beta}(\lambda_N)\rangle\langle\varphi_a^{\beta}(\lambda_N)|\widehat{\mathbf{H}}_u^{\mathbf{SO}}|\varphi_k^{\beta}(\lambda_N)\rangle}{\varepsilon_k - \varepsilon_a}\right] \quad \text{(S1)}$$

In this work, the $\sigma^{SO/FC}$ is calculated using the finite-field perturbation theory in combination with SOS-DFPT approach[1] as given in formula S1. In formula S1, the Fermi-contact operator is introduced as a finite-field perturbation (λ_N) leading to different (α) and (β) electron orbital functions (φ), and, hence different matrix elements of the spin-orbit ($\widehat{H}^{SO}$) and angular momentum ($\hat{l}_v$) operator in S1. The summations go through occupied (occ) and virtual (virt) orbitals and the coefficients (ε) in denominators are the corresponding orbital energies.

Table S1: σ^{SO}(N1) and σ^{SO}(C2') in compounds **1-12** calculated using MAG and ADF, s-character of the light atom and d-character of the heavy metal atom in the M-LA bonding. σ^{SO}(LA) in ppm, s- and d-character in %.

N1	**1**	**2**	**3**	**4**	**5**	**6**	**7**	**8**	**9**	**10**	**11**	**12**
σ^{SO} MAG [a]	**34.1**	**28.2**	17.2	27.5	**10.6**	**-17.8**	6.0	-6.5	1.5	-11.8	4.4	-16.7
σ^{SO} ADF [b]	**42.2**	**30.1**	26.1	31.6	**20.7**	**-15.3**	13.6	-6.7	7.7	-11.6	7.7	-16.4
s-character LA [c]	**29**	**28**	29	29	**27**	**26**	26	27	27	26	27	26
d-character M [c]	**56**	**54**	52	55	**56**	**48**	54	50	52	49	52	48
C2´												
σ^{SO} MAG [a]	**37.0**	**42.5**	38.9	34.0	**-5.5**	**20.9**	20.5	-5.2	-4.0	9.9	-5.0	14.2
σ^{SO} ADF [b]	**31.5**	**35.0**	40.6	28.3	**-8.0**	**18.9**	20.6	6.4	-7.0	9.9	-8.0	15.4
s-character LA [c]	**28**	**29**	29	28	**26**	**27**	25	28	26	26	26	26
d-character M [c]	**52**	**54**	55	52	**49**	**57**	56	54	51	55	52	55

[a] PBE/def2-TZVP/def2-SVP; [b] PBE-40/TZP/SO-ZORA; [c] PBE-40/TZP/ZORA.

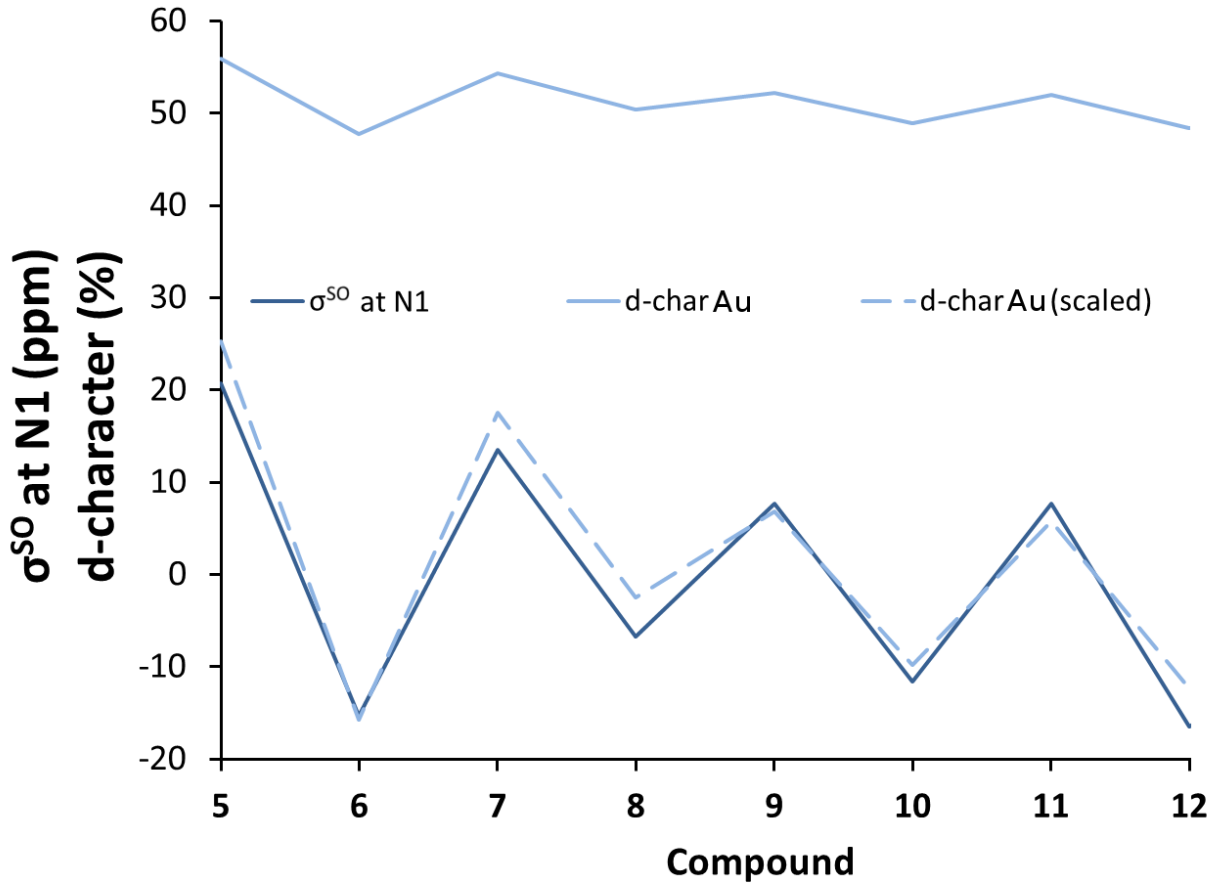

Figure S1: σ^{SO} at N1 (calculated at PBE0-40/TZP/SO-ZORA level). The dashed line represents the Au d-character in the Au–N bond (calculated at PBE0-40/TZP/SR-ZORA level) uniformly scaled [(d-char - 51)*5] to overlap with σ^{SO} at N1.

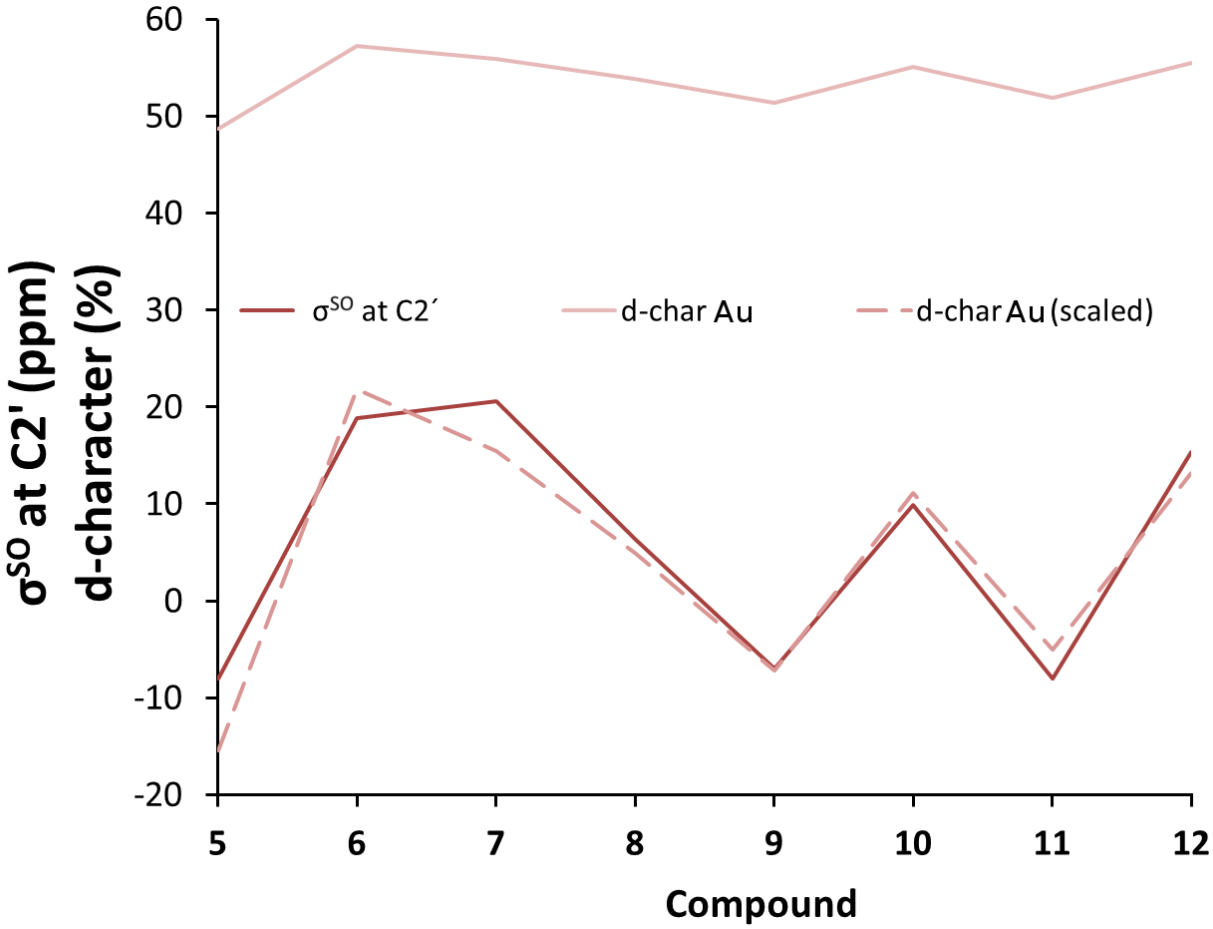

Figure S2: σ^{SO} at C2' (calculated at PBE0-40/TZP/SO-ZORA level) for compounds **1-12**.. The dashed line represents the Au d-character in the Au–C2' bond (calculated at PBE0-40/TZP/SR-ZORA level) uniformly scaled [(d-char - 53)*5] to overlap with σ^{SO} at N1.

Table S2: Total σ^{SO}(N1) and σ^{SO}(C2'), MO contributions to σ^{SO}(N1) and σ^{SO}(C2'), tensor components, and relative portion of individual metal AOs in total metal contribution to MO for **1-12.**

Compound		Total σ^{SO} (ppm)	MO	σ^{SO} MOs (ppm)	σ^{SO} tensor components (ppm)			Relative metal contribution (%)		
					xx	yy	zz	5d	6s	6p
1	N1	34.1	56	11.9	-1.6	1.3	35.9	98.4	1.6	0.0
			59	26.0	-9.0	72.5	14.6	98.4	0.0	1.6
	C2'	37.0	56	22.0	1.4	3.3	61.2	98.4	1.6	0.0
			58	12.9	-3.4	41.7	0.5	100.0	0.0	0.0
2	N1	28.2	56	25.2	-1.1	67.5	9.1	100.0	0.0	0.0
	C2'	42.5	57	19.3	2.1	1.1	54.1	96.5	3.5	0.0
			59	19.5	-0.4	55.2	3.1	100.0	0.0	0.0
3	N1	17.2	63	17.7	-9.8	47.5	15.1	96.4	0.0	3.6
	C2'	38.9	60	17.1	2.1	4.1	43.8	97.7	2.3	0.0
			62	16.7	-1.9	51.5	0.4	100.0	0.0	0.0
4	N1	27.5	60	25.0	-0.1	67.4	7.1	100.0	0.0	0.0
	C2'	34.0	56	15.8	-0.4	0.1	47.6	100.0	0.0	0.0
			61	10.0	2.1	2.1	24.1	92.5	7.5	0.0
			63	13.5	-0.3	37.6	3.1	100.0	0.0	0.0
5	N1	10.6	52	3.2	0.7	-6.8	15.7	100.0	0.0	0.0
			55	3.1	0.1	0.0	9.3	87.5	0.0	12.5
			58	3.1	1.7	2.7	5.0	100.0	0.0	0.0
	C2'	-5.5	43	9.7	-0.2	-1.0	30.1	100.0	0.0	0.0
			55	2.6	3.1	-0.6	6.0	87.5	0.0	12.5
			59	-18.1	-40.3	1.0	-15.1	37.5	0.0	62.5
6	N1	-17.8	55	-8.4	0.5	-19.5	-18.5	39.3	50.0	10.7
			54	-12.5	-45.9	-5.1	25.1	60.0	25.0	15.0
	C2'	20.9	48	7.6	0.3	22.1	0.2	100.0	0.0	0.0
			50	10.6	-0.1	0.5	31.1	100.0	0.0	0.0
7	N1	6.0	57	7.6	0.3	15.1	7.1	100.0	0.0	0.0
	C2'	20.5	44	19.8	-0.8	-0.5	60.7	100.0	0.0	0.0
8	N1	-6.5	55	18.0	72.4	-5.9	-12.4	93.7	6.3	0.0

			56	-24.4	-52.0	2.1	-23.9	54.7	41.5	3.8
	C2’	-5.2	41	3.6	-1.4	-0.3	12.1	92.3	7.7	0.0
			52	2.1	4.0	-2.4	4.1	98.1	0.0	1.9
			53	4.5	-5.8	2.1	16.1	98.0	0.0	2.00
			57	3.1	5.1	0.3	3.1	100.0	0.0	0.0
			59	-18.6	-37.7	0.2	-18.4	0.0	0.0	100.0
9	N1	1.5	61	2.7	1.1	3.1	3.1	100.0	0.0	0.0
	C2’	-4.0	53	13.4	-0.1	3.1	36.7	81.3	0.0	18.7
			60	7.3	11.1	-1.0	11.1	60.0	0.0	40.0
			63	-23.7	-50.2	1.1	-22.3	37.5	12.5	50.0
10	N1	-11.8	56	14.8	20.1	-9.4	32.9	100.0	0.0	0.0
			58	-27.6	-53.6	11.1	-40.9	52.9	29.4	17.7
	C2’	9.9	54	11.4	-0.2	0.3	34.1	100.0	0.0	0.0
11	N1	4.4	57	4.3	1.1	2.1	9.1	92.3	0.0	7.7
	C2’	-5.0	48	6.9	-8.1	19.1	8.1	100.0	0.0	0.0
			57	4.5	2.1	0.7	10.1	92.3	0.0	7.7
			61	-19.3	-40.7	-0.2	-17.1	0.0	14.3	85.7
12	N1	-16.7	57	-27.3	-48.6	-39.9	6.1	57.7	34.6	7.7
	C2’	14.2	51	11.8	-0.1	-0.4	35.8	100.0	0.0	0.0

Table S3: Total σ^{SO}(N1) and σ^{SO}(C2'), MO contributions to the σ^{SO}(N1) and σ^{SO}(C2'), and absolute contributions of individual AOs of metal to a given MO for **1**, **2**, **5**, and **6**.

N1	Total σ^{SO}	MO	σ^{SO} MOs (ppm)	Absolute contribution of metal AO to MO		
				5d	6s	6p
1	34.1	56	11.9	0.61	0.01	0.00
		59	26.0	0.61	0.00	0.01
2	28.2	56	25.2	0.69	0.00	0.00
5	10.6	52	3.2	0.17	0.00	0.00
		55	3.1	0.21	0.00	0.03
		58	3.1	0.09	0.00	0.00
6	-17.8	54	-12.5	0.11	0.14	0.03
		55	-8.4	0.12	0.05	0.03
C2´						
1	37.0	56	22.0	0.61	0.01	0.00
		58	12.9	0.45	0.00	0.00
2	42.5	57	19.3	0.55	0.02	0.00
		59	19.5	0.51	0.00	0.00
5	-5.5	43	9.7	0.33	0.00	0.00
		55	2.6	0.21	0.00	0.03
		59	-18.1	0.03	0.00	0.05
6	20.9	48	7.6	0.58	0.00	0.00
		50	10.6	0.32	0.00	0.00

Table S4: Total σ^{SO}(LA), occupied MO (MO) and vacant MO (MO*), σ^{SO} contribution of particular MO→MO* magnetic coupling, energy difference between MO and MO*, and absolute contributions of individual metal AOs to MO* for **1-12**. NMR shielding in ppm, energy difference in a.u.

Compound	Atom	Total σ^{SO}	MO	MO*	σ^{SO} for given MO→MO*	Energy difference	Absolute contribution of metal AO to MO*		
							5d	6s	6p
1	N1	34.1	56	63	18.8	4.93	0.41	0.08	0.00
			59	63	29.7	4.38	0.41	0.08	0.00
	C2’	37.0	56	63	38.1	4.93	0.41	0.08	0.00
			58	63	5.4	4.64	0.41	0.08	0.00
				64	3.6	4.83	0.06	0.07	0.11
				71	5.0	7.14	0.10	0.72	0.15
2	N1	28.2	56	63	28.4	5.12	0.33	0.06	0.03
	C2’	42.5	57	63	28.3	4.95	0.33	0.06	0.03
			59	63	7.1	4.13	0.33	0.06	0.03
				65	8.7	4.56	0.14	0.07	0.07
				71	6.4	6.61	0.02	0.59	0.19
3	N1	17.2	63	66	20.4	4.13	0.41	0.04	0.02
	C2’	38.9	60	66	9.7	4.56	0.41	0.04	0.02
				68	5.1	5.00	0.01	0.12	0.08
			62	66	12.3	4.30	0.41	0.04	0.02
				114	5.9	17.93	0.22	0.00	0.04
4	N1	27.5	60	67	26.0	4.88	0.39	0.04	0.02
	C2’	34.0	56	67	18.9	6.00	0.39	0.04	0.02
			61	67	13.4	4.68	0.39	0.04	0.02
			63	67	6.3	3.98	0.39	0.04	0.02
5	N1	10.6	52	62	8.2	6.15	0.35	0.12	0.00
				78	3.7	11.69	0.01	0.00	0.00
				80	-7.5	12.28	0.01	0.01	0.00
			55	62	3.3	4.82	0.35	0.12	0.00
			58	62	2.0	4.25	0.35	0.12	0.00
	C2’	-5.5	43	62	13.1	7.95	0.35	0.12	0.00
				135	-3.1	27.88	0.02	0.00	0.00

			55	68	1.4	7.71	0.05	0.34	0.00
				79	2.1	10.74	0.00	0.04	0.07
			59	63	-1.6	4.30	0.00	0.00	0.06
				66	-6.2	6.02	0.00	0.00	0.85
				76	-1.9	8.74	0.01	0.00	0.01
				87	-2.9	11.83	0.03	0.00	0.00
				107	-1.5	17.36	0.10	0.00	0.01
				112	-3.7	18.06	0.02	0.00	0.22
				139	-1.9	24.51	0.08	0.00	0.05
6	N1	-17.8	55	77	-3.7	10.43	0.02	0.00	0.00
				94	-6.0	15.8	0.18	0.00	0.01
			54	66	-3.9	7.70	0.00	0.00	0.87
				83	-2.2	12.38	0.00	0.03	0.00
				108	-3.1	22.36	0.00	0.00	0.24
				121	-3.2	19.14	0.01	0.00	0.17
	C2’	20.9	48	63	9.5	7.49	0.30	0.00	0.03
			50	63	11.8	6.71	0.30	0.00	0.03
7	N1	6.0	57	62	5.3	4.27	0.39	0.03	0.02
	C2’	20.5	44	62	25.1	7.69	0.39	0.03	0.02
8	N1	-6.5	55	63	31.4	6.45	0.22	0.06	0.01
				91	-12.0	14.38	0.06	0.00	0.00
			56	62	-2.6	5.69	0.00	0.00	0.07
				66	-5.6	7.28	0.00	0.00	0.79
				76	-3.5	10.00	0.00	0.00	0.02
				79	-1.7	10.37	0.00	0.01	0.03
				91	-3.7	13.92	0.06	0.00	0.00
				106	-2.3	17.90	0.32	0.23	0.01
				111	-2.8	18.79	0.02	0.00	0.19
				185	-1.7	42.04	0.03	0.00	0.00
	C2’	-5.2	41	63	6.6	9.30	0.22	0.06	0.01
				91	-2.8	17.22	0.06	0.00	0.00
			52	83	5.4	12.24	0.11	0.28	0.05
				84	-2.5	12.44	0.00	0.02	0.08
			53	63	4.5	6.80	0.22	0.06	0.01

			57	60	0.7	3.39	0.01	0.00	0.02
				63	0.9	5.49	0.22	0.06	0.01
				67	0.7	7.13	0.06	0.55	0.13
				95	0.7	14.77	0.58	0.00	0.00
			59	62	-2.3	4.44	0.00	0.00	0.07
				63	-4.1	4.74	0.22	0.06	0.01
				65	-3.8	5.96	0.00	0.08	0.10
				86	-2.2	10.95	0.00	0.08	0.02
				90	-2.4	12.02	0.05	0.00	0.00
				116	-2.3	18.35	0.00	0.01	0.00
9	N1	1.5	61	66	2.1	3.97	0.28	0.10	0.00
	C2’	-4.0	53	66	7.3	6.20	0.28	0.10	0.00
				84	2.6	12.4	0.11	0.25	0.00
				93	2.5	15.49	0.01	0.00	0.00
			60	90	1.8	12.32	0.00	0.00	0.01
				96	2.5	14.53	0.00	0.00	0.01
				115	2.5	18.78	0.08	0.01	0.00
			63	70	-7.6	6.00	0.00	0.00	0.84
				96	-2.1	13.59	0.00	0.00	0.01
				91	-2.9	11.85	0.03	0.00	0.00
				113	-2.9	17.53	0.02	0.00	0.31
				114	-4.1	17.68	0.06	0.00	0.05
				116	-3.5	17.98	0.02	0.00	0.15
10	N1	-11.8	56	92	4.8	14.54	0.00	0.04	0.10
				190	8.3	44.74	0.06	0.03	0.08
			58	70	-6.9	7.70	0.01	0.53	0.59
				112	-6.5	19.07	0.01	0.12	0.12
				80	-6.0	10.41	0.00	0.00	0.30
				81	-4.2	10.59	0.00	0.00	0.02
				87	-3.9	12.35	0.00	0.00	0.29
	C2’	9.9	54	66	12.7	6.42	0.24	0.00	0.00
11	N1	4.4	57	64	3.7	5.69	0.25	0.03	0.05
	C2’	-5.0	48	67	3.6	9.08	0.00	0.00	0.52
				121	4.1	23.57	0.21	0.03	0.00

			57	64	4.5	5.69	0.25	0.03	0.05
			61	64	-3.3	4.43	0.25	0.03	0.05
				65	-3.4	4.58	0.00	0.00	0.10
				67	-5.0	5.78	0.00	0.00	0.52
				80	-1.9	9.09	0.00	0.01	0.01
				113	-1.5	17.83	0.00	0.00	0.26
				115	-1.7	18.32	0.00	0.00	0.08
				117	-2.0	19.08	0.04	0.00	0.00
12	N1	-16.7	57	64	-3.0	5.22	0.25	0.00	0.02
				67	-7.1	7.48	0.00	0.00	0.83
				75	-3.8	9.50	0.03	0.15	0.57
				78	-4.5	10.26	0.00	0.21	0.25
				113	-4.6	19.16	0.00	0.00	0.30
				189	-3.8	43.98	0.52	0.00	0.00
	C2’	14.2	51	64	13.7	6.08	0.25	0.00	0.02

EHT calculations and bonding analysis

Computational details. Extended Hückel Theory calculations and their graphical output in the form of the interaction diagrams and MO plots have been performed by means of the C.A.C.A.O. program[2] employing the default values of EHT parameters for all atoms involved. Relativistic effects are not accounted for explicitly within this approach; however, scalar relativity as influencing atomic orbital energies and radii is approximately included via the semiempirical parameters. Same input structures and molecular orientations in the cartesian coordinate system were used as for the DFT calculations reported in the main text except for neglecting the tiny distortions of the molecule from the Cs symmetry.

Bonds subject to analysis. Since in a qualitative analysis of bonding, the most simple models often appear as the most illuminating ones,[3,4] we decided for a minimum model of bonding represented by three occupied bonding molecular orbitals (MOs) representing the three Pt(Au)-C and Pt(Au)-N bonds. The fourth bond, between Pt(Au) and F, is below disconsidered from the discussions of covalent interactions due its separability from the rest of the bonds and a higher ionicity. Indeed, the interactions between Pt(Au) and F are largely separated from the rest of the interactions and the total overlap populations (OPs) do not exceed the values of 0.20, 0.17, 0.20, and 0.18 for complexes **1**, **2**, **5**, and **6**, respectively. At the same time, the interactions between Pt(Au) and C(N) strongly mix with each other and the sum of all corresponding OPs is 0.92, 0.99, 1.08, and 1.07 for complexes **1**, **2**, **5**, **6**, respectively.

FMO selection procedure. The analysis of most important metal-ligand orbital interactions is in the C.A.C.A.O. package aided by the fragment analysis. Molecular orbitals of compounds can be built from MOs of a fragment 1, composed in our case by all ligand atoms, and of a fragment 2, represented in our case by the transition metal. Molecular orbitals of both fragments are denoted as fragment molecular orbitals (FMOs) and are numbered in the order of the fragment number and a decreasing energy. The fragment analysis enables the evaluation of

contributions of all pairs of FMOs into the total OP. **Table S4.5** displays seven most important contributions of FMO pairs as found for complexes **1**, **2**, **5**, and **6**. Fragment MOs 69, 70, 71, and 73 entering at the second position of the matrix elements belong to fragment 2 (Pt^{2+}/Au^{3+}) and represent the empty atomic orbitals $6p_y$, $6p_x$, 6s, and $5d_{x2-y2}$, respectively. In order to obtain as a result three occupied MOs, we need to consider for each compound three occupied ligand FMOs. **Table S4.5** demonstrates that, indeed, dominant OP contributions of at least 0.08 are in all cases due to three FMOs of the ligand fragment 1: FMOs 31, 33, and 39 for **1**; FMOs 31, 32, and 39 for **2**; FMOs 31, 32, and 33 for **5** and **6**. Consequently, for each of the compounds, seven FMOs in total are considered, summarized in the columns of **Table S4.5** after disregarding the fluorine FMO 67.

Table S4.5 Most important contributions of FMO pairs as found for complexes **1**, **2**, **5**, and **6**[a]

Overlap populations for FMOs × 100							
1		**2**		**5**		**6**	
FMO pair	contrib.	FMO pair	contrib.	FMO pair	contrib.	FMO pair	contrib.
⟨31|73⟩	21	⟨31|73⟩	22	⟨32|69⟩	26	⟨32|71⟩	26
⟨39|69⟩	16	⟨39|70⟩	16	⟨31|69⟩	20	⟨31|73⟩	25
⟨31|69⟩	15	⟨31|69⟩	15	⟨31|73⟩	14	⟨32|70⟩	20
⟨31|71⟩	10	⟨39|71⟩	11	⟨33|71⟩	13	⟨33|70⟩	10
⟨33|70⟩	8	⟨32|70⟩	9	⟨32|73⟩	13	⟨31|69⟩	9
⟨33|71⟩	7	⟨31|71⟩	9	⟨33|70⟩	8	⟨33|71⟩	7
⟨67|70⟩	7	⟨32|71⟩	7	⟨67|70⟩	8	⟨67|69⟩	7
⟨39|71⟩	6	⟨39|73⟩	6	⟨31|71⟩	7	⟨53|69⟩	5

[a] FMO 31-67 correspond to fragment 1, with FMOs 31, 32, 33, 39 responsible for bonds to C and N and FMO 67 responsible for bond to F. FMOs 69, 70, 71, and 73 belong to fragment 2 (metal) and represent the empty atomic orbitals $6p_y$, $6p_x$, 6s, and $5d_{x2-y2}$, respectively. The numbering of FMOs is (1) in the order of fragment number and (2) in the order of decrasing energy.

MO selection procedure. Fragment molecular orbitals described above in principle contribute to all MOs accessible by the a' symmetry. Therefore, a scheme must be established to identify the three desired occupied bonding MOs. For our purpose of linking SO-HALA contributions to chemical shift to covalence, is natural to identify three occupied MOs that contribute most extensively to the metal-ligand bonding. Unfortunately, while for some MOs such identification turned out to be unique, for other it was to some extent arbitrary and a rationalized choice described below had to be done.

Bonding MOs for complex 1. For compound **1**, FMO 31 donates electrons to FMO 73 (most), 69 (less), and 71 (least), cf. **Table S4.5**. We thus seek for MO a single MO that would have, at best, significant contributions of all of FMOs 31, 73, 69, and 71. Mulliken population reveals that such MO is doubtless MO 41 shown in **Figure S2.5**, which is the first most contributed occupied MO by FMO 31 and FMO 69 and the second most contributed occupied MO by FMO 73. MO 41 contains less than 0.5% of FMO 71, hence electron donation from FMO 31 to FMO 71 could only be described by an inclusion of an additional MO and we neglect it in order to keep the model simple. Fragment orbital FMO 39 donates electrons into FMO 69 (**Table S4.5**), and the best corresponding MO of choice is doubtless MO 51 (see **Figure S2.5**) which is the first most contributed occupied MO by FMO 39 and the second most contributed occupied MO by FMO 69.

The donation from FMO 33 into FMOs 70 and 71 can be described by either MO 36 (14% of FMO 33, 7% of FMO 71), MO 42 (43% of FMO 33, 1% of FMO 70), or MO 45 (16% of FMO 33, 1% of FMO 70, 1% of FMO 71) displayed in **Figure S2.5**. While MO 36 corresponds to a weak π interaction and MO 42 to a hybrid σ-π interaction between Pt and the aromatic rings, MO 45 represents the most efficient bonding of the pyridine nitrogen. Since MO 41 describes bonding to aromatic C and MO 51 bonding to the ammonia, we select as a third MO orbital 45 in order to describe as efficiently as possible bonding to the aromatic N. Covalent bonding to C and

N in **1** is thus below described through MOs 41, 45, and 51 with an interaction diagram displayed in **Figure S3a,** which additionally displays the lowest lying empty antibonding MO falling within the energy range covered by selected metal AOs. The compositions of selected MOs are listed in **Table S5**. Interaction diagrams given below have been constructed without magnifying energy differences between quasi-degenerate levels and all fragment molecular orbital (FMO) contribution thresholds have been kept at their default value (2 %).

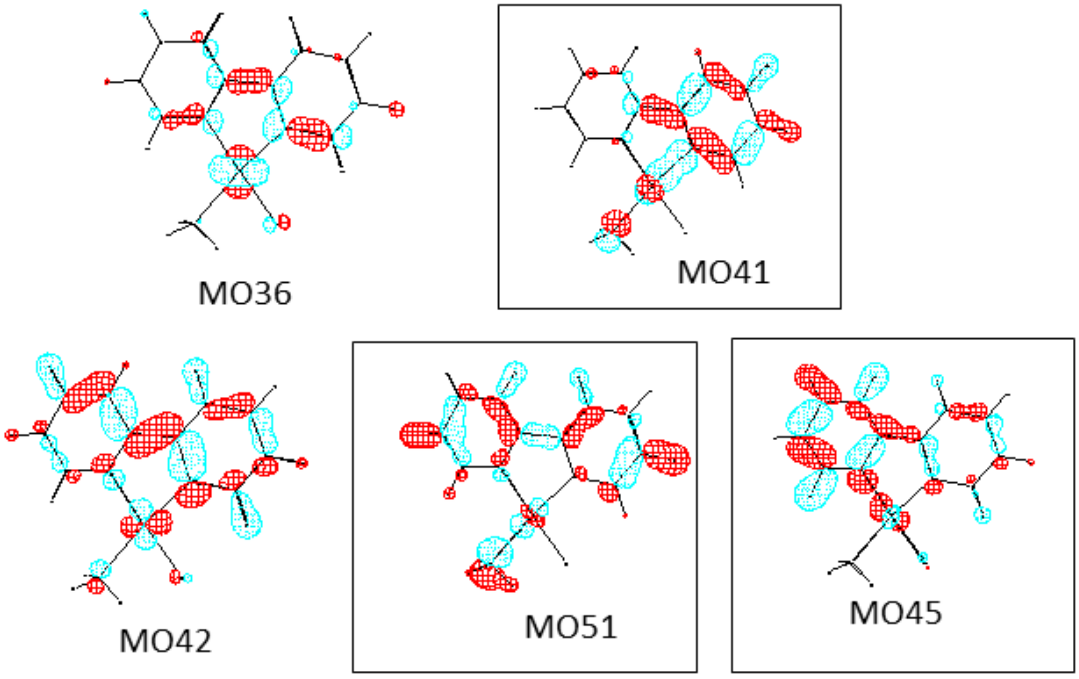

Figure S2.5 Composition of MOs 36-51 of compound **1** discussed in text. Orbitals in frames were selected for the description of the two Pt-N and the one Pt-C bond and their composition is analyzed in **Figure S3**.

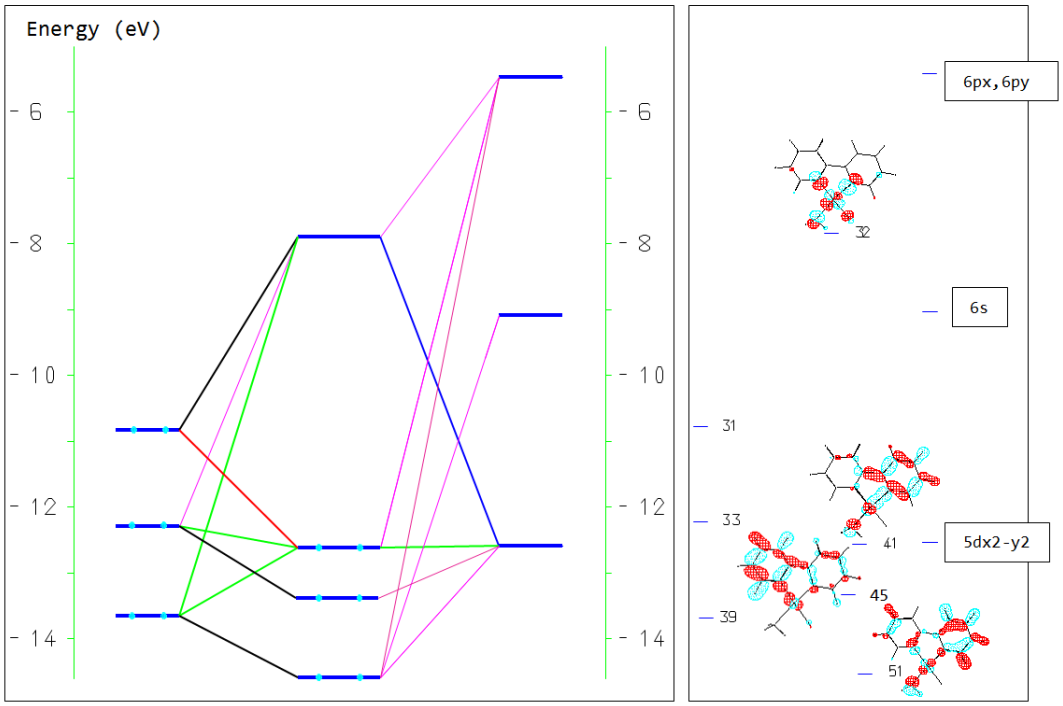

a)

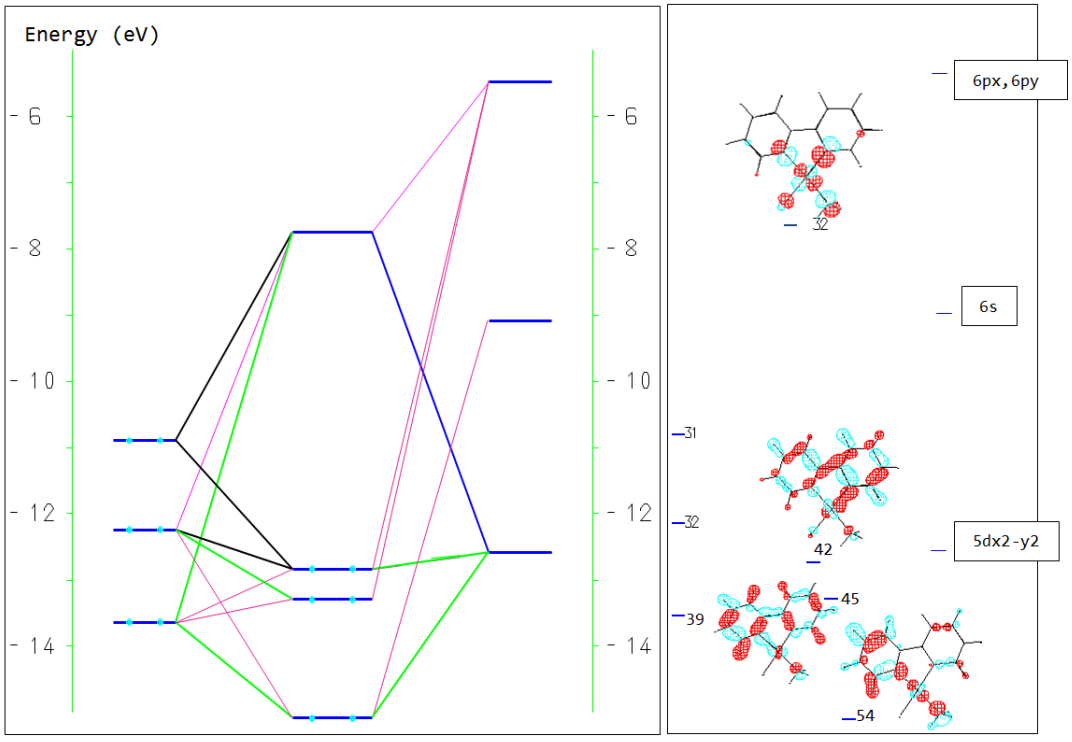

b)

Figure S3. Interaction diagram of compounds (a) **1** and (b) **2** for fragment orbitals providing contributions to the overlap population of at least 0.08. The contributions of selected FMOs to MOs are indicated by the color code: pink − 2 to 5 %, green − 6 to 15 %, black – 16 to 30 %, red – 31 to 50 %, blue – 51 to 75%, magenta – 76 to 100%. Cf. also **Table S5**.

Extended legend for Figures S3 and S4. The right frame contains on its left side energy levels and FMO numbers (numbering starting from highest energy) for the ligand and on its right side energy levels and AO labels for the metal. In the middle, energy levels, MO numbers and MO plots are given for the three most important occupied plus the lowest unoccupied level resulting from the interaction between the two sets of FMOs. The left frame repeats on it left side, right side, and in the middle the energy levels for fragments 1, 2, and the whole complex, respectively. These are connected with the individual FMO levels according to the percentual participation of an FMO in a MO using the color code: below 2% - no line, 2 to 5% - pink, 6 to 15% - green, 16 to 30% - black, 31 to 50% - red, 51 to 75% - blue.

Table S5. Contributions of all metal AOs into occupied MOs plotted in Figures S3 and S4.[a]

Complex	MO	dxy	dz2	dx2-y2	s	px	py
1	**41**	**0**	**19**	**7**	**0**	**0**	**5**
	45	**1**	**4**	**2**	**1**	**1**	**0**
	51	**0**	**2**	**4**	**2**	**0**	**2**
2	**42**	**4**	**4**	**12**	**0**	**1**	**2**
	45	**2**	**2**	**1**	**0**	**3**	**0**
	54	**1**	**2**	**8**	**2**	**0**	**0**
5	**36**	**0**	**0**	**1**	**0**	**0**	**15**
	41	**0**	**1**	**0**	**6**	**1**	**0**
	54	**5**	**12**	**20**	**0**	**0**	**0**
6	**39**	**0**	**1**	**2**	**7**	**5**	**2**
	40	**2**	**0**	**3**	**2**	**1**	**1**
	55	**1**	**20**	**17**	**1**	**0**	**0**

[a]MO compositions given refer to gross Mulliken populations of corresponding AOs, with the threshold value set to 0.5%.

Bonding MOs for complex 2. For compound **2**, FMO 31 donates electrons to FMO 73 (most), 69 (less), and 71 (least), cf. **Table S4.5**. This scheme is identical to the one obtained for compound **1**. We thus seek for MO a single MO that would have, at best, significant

contributions of all of FMOs 31, 73, 69, and 71. Mulliken population reveals that such MO is doubtless MO 42 shown in **Figure S3.5**, which is the first most contributed occupied MO by FMOs 31 and 73 and also, along with MOs 41 and 76, the most contributed occupied MO by FMO 69. Molecular orbital 42 contains less than 0.5% of FMO 71, hence electron donation from FMO 31 to FMO 71 could only be described by an inclusion of an additional MO and we neglect it in order to keep the model simple.

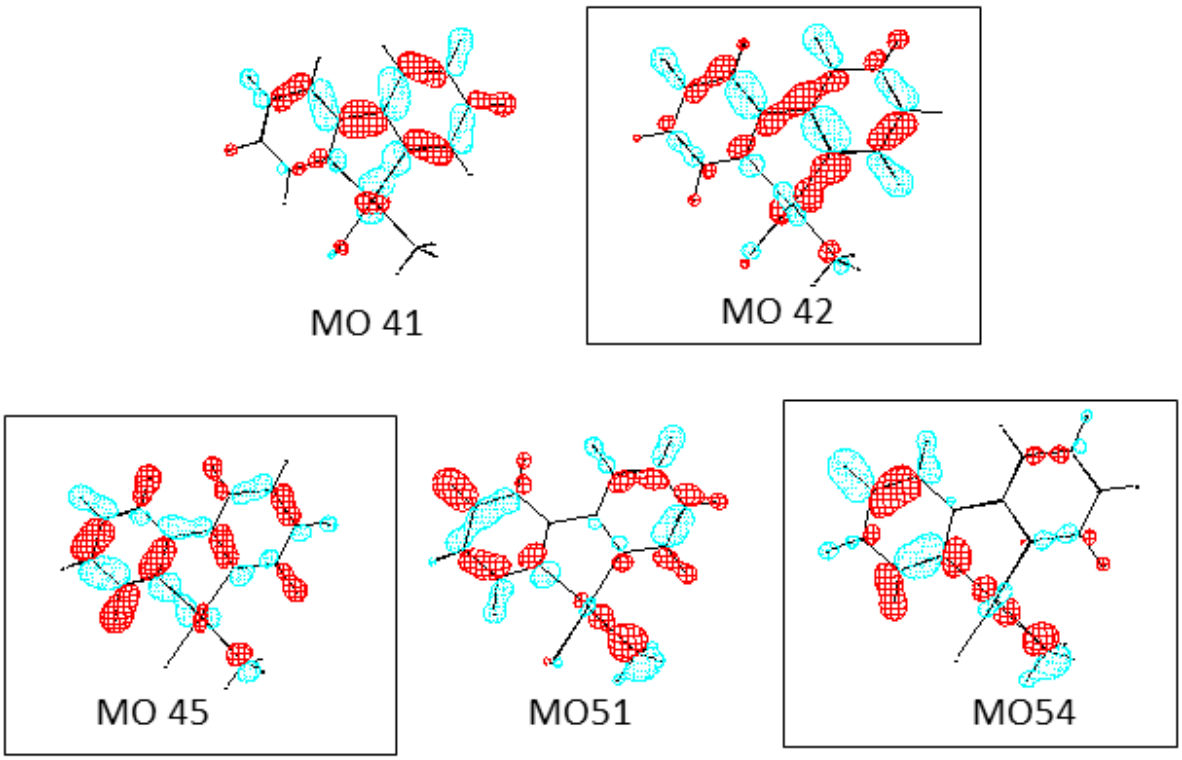

Figure S3.5 Composition of MOs 41 -54 of compound 2 discussed in text. Orbitals in frames were selected for the description of the two Pt-N and the one Pt-C bond and their composition is analyzed in Figure S3.

Fragment orbital FMO 39, unlike in compound **1**, donates in compound **2** electrons into FMOs 70, 71, and 73 (**Table S4.5**). This donation can be described by either MO 51 (22% of FMO 39, 4% of FMO 70, 1% of FMO 71, 1% of FMO 73), or by MO 54 (13% of FMO 39, 2%

of FMO 71, 8% of FMO 73) displayed in **Figure S3.5**. Of these, the latter MO 54 contains more metal character and thus covers a larger portion of covalent bonding. Hence we employ MO 54 to describe bonding through FMO 39. The donation from FMO 32 into FMOs 70 and 71 can be described by either MO 41 (35% of FMO 32, 1% of FMO 70), MO 42 (23% of FMO 32, 1% of FMO 70), or MO 45 (14% of FMO 32, 3% of FMO 70), displayed in **Figure S3.5**. While MO 42 was already employed for bonding via FMO 31 (cf. above), out of MOs 41 and 45, the latter described a higher portion of the FMO 39 → FMO 70 charge transfer (since the coefficient of FMO 70 is three times larger in MO 45 than in MO 41). Covalent bonding to C and N in **1** is thus below described through MOs 42, 45, and 54 with an interaction diagram displayed in **Figure S3b.**

Bonding MOs for complex 5. For compound **5**, unlike for **1** and **2**, the highest individual electron donation comes from FMO 32 (rather than 31) which donates electrons to FMOs 69 and 73 (two times less), cf. **Table S4.5**. Molecular orbital possessing significant contributions of FMOs 32 and 69 is MO 36 shown in **Figure S3.7** which is the first most contributed occupied MO by both FMO 32 (34%) and FMO 69 (15%) and contains also FMO 73 (1%). FMO 31 donates electrons to FMOs 69, 73, and 71. Excluding MO 36 which was already selected above, the second most donated orbital by FMO 31 is MO 54 (4% FMO 31) which is also MO most contributed by FMO 73 (20%). Finally, FMO 33 contributes strongly to MOs 38 (57%) and 41 (21%), see **Figure S3.7**, and the same is valid for FMO 71 which is the most strongly FMO coupled to FMO 33 (participation of FMO 71 of 2% in MO 38 and of 6% in MO 41). Since we look for significantly covalent MOs, we select as the third orbital MO 41 for which the contributions of FMOs 33 and 71 are more balanced and which has an "intra-bond" character, unlike MO 38, which is of a "inter-bond" character, cf. Figure S3.7.

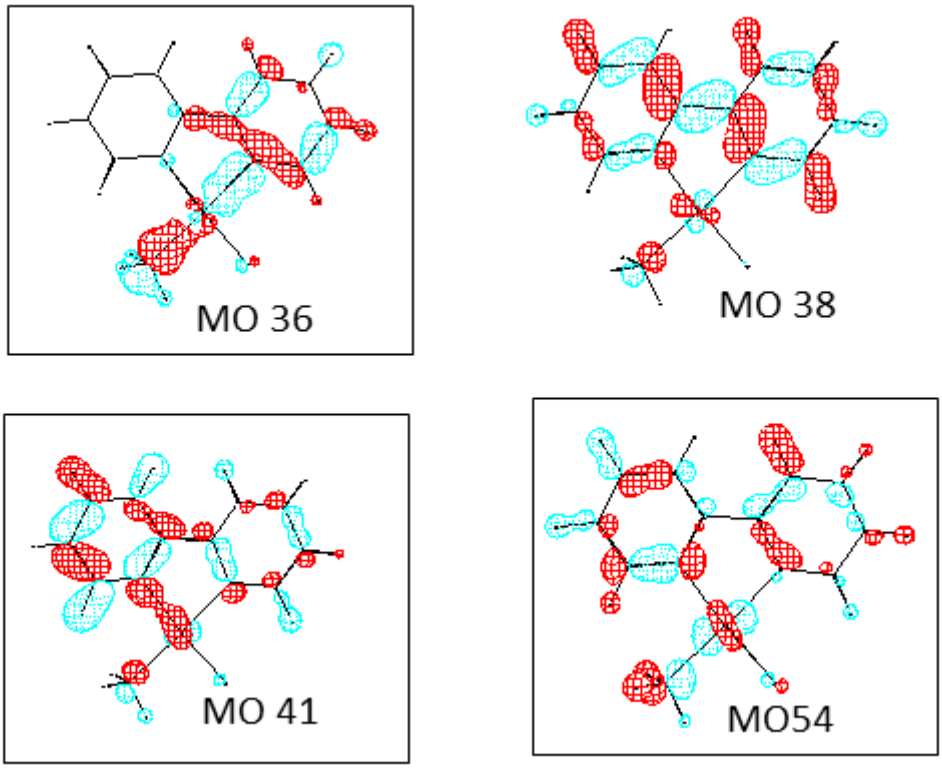

Figure S3.7 Composition of MOs 36 -54 of compound 5 discussed in text. Orbitals in frames were selected for the description of the one Au-N and the two Au-C bond and their composition is analyzed in Figure S4.

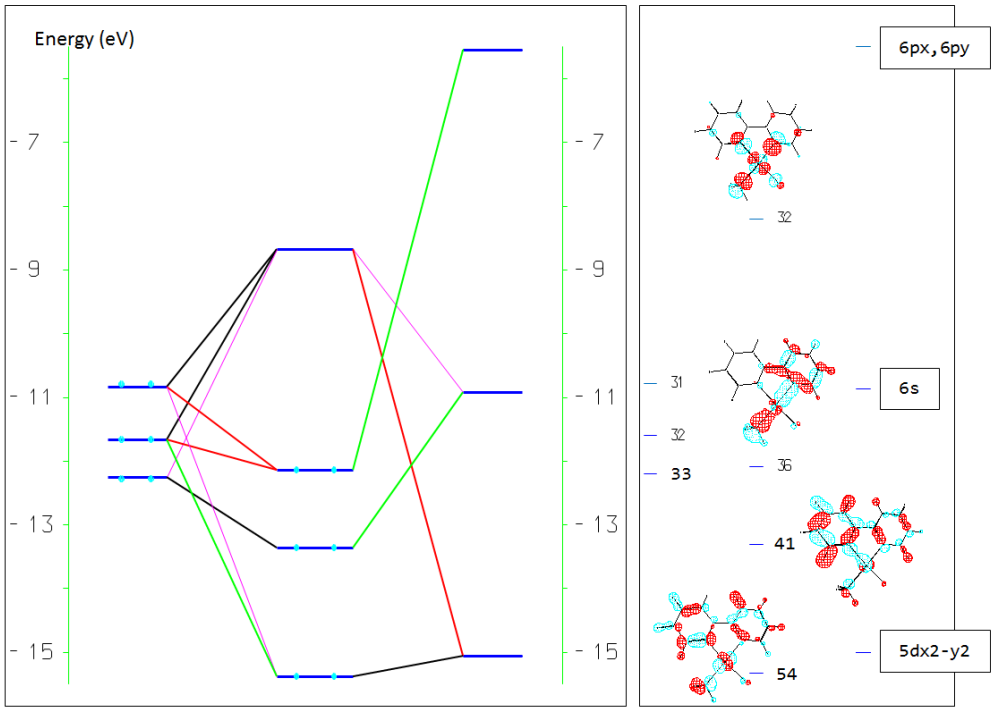

a)

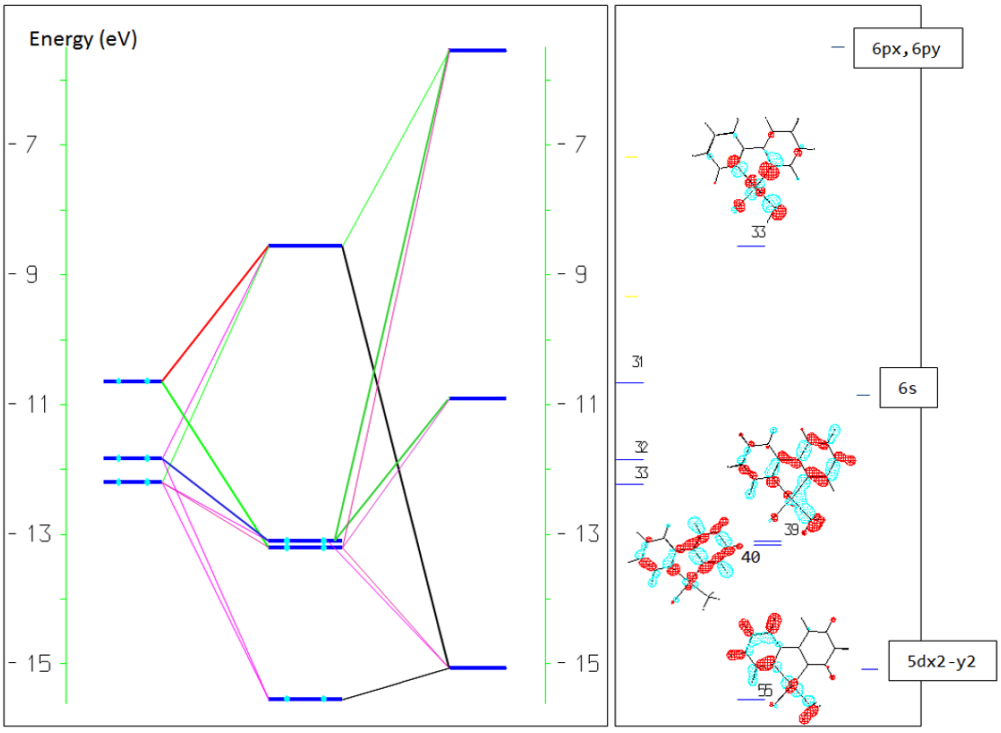

b)

Figure S4. Interaction diagram of compounds (a) **5** and (b) **6** for fragment orbitals providing contributions to the overlap population of at least 0.08. The contributions of selected FMOs to MOs are indicated by the color code: pink − 2 to 5 %, green − 6 to 15 %, black – 16 to 30 %, red – 31 to 50 %, blue – 51 to 75%, magenta – 76 to 100%. Cf. also **Table S5**.

Bonding MOs for complex 6. For compound **6**, like for **5**, the highest individual electron donation comes from FMO 32 which, unlike in **5**, donates electrons predominantly to FMOs 71 and 70 cf. **Table S4.5**. Molecular orbital possessing the largest contribution of FMO 32 is MO 39 (56% of FMO 32) which contains also 7% (5%) of FMO 71 (FMO 70). To describe donation from FMO 31, the most appropriate occupied MO is 40, which contains also 3%, 2%, and 1% of FMOs 73, 71, and 70, respectively. Finally, FMO 33 contributes strongly to MOs 37 (74%), 40 (3%), and 55 (4%). The admixtures of FMO 70 and 71 into these MOs are small, however, MO 55 contains 17% of FMO 73 which is the metal d_{x2-y2} AO, very suitable for bonding. Thus, the three MOs 39, 40, and 55 plotted in **Figure S4.5** seem to be the most suitable to describe the mutually coupled interactions of individual fragment molecular orbitals.

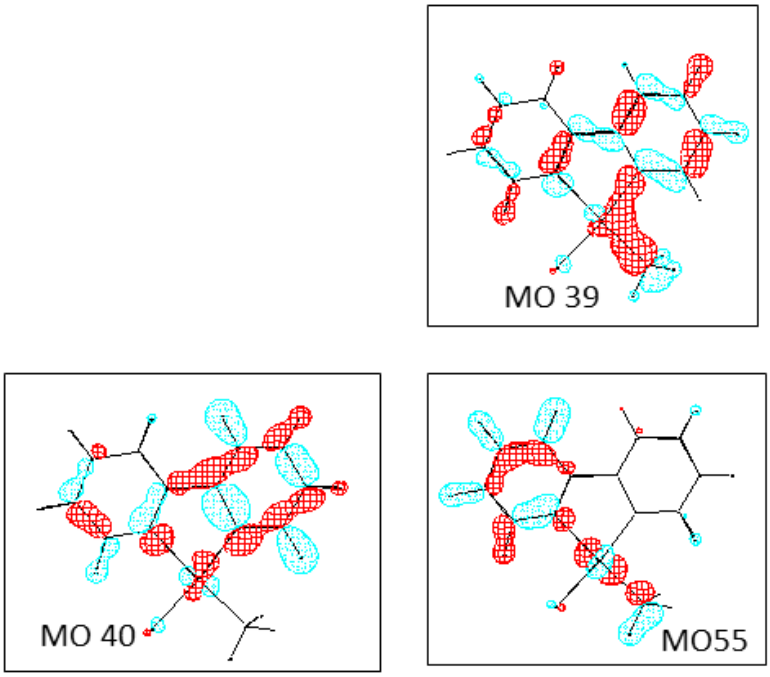

Figure S4.5 Composition of MOs 39 -55 of compound 6 discussed in text. Orbitals in frames were selected for the description of the one Au-N and the two Au-C bond and their composition is analyzed in Figure S4

The dependence of s, p, and d character of bonding MOs on MO selection criteria. As is apparent from the previous discussion, the selection procedure for bonding MOs suggests in some cases several possibilities out of which an arbitrary choice has to be made. This is to some extent a necessary prize for keeping only a few orbitals in the bonding picture. We have therefore employed also a different MO choice for which MOs were strictly determined by a maximization of product of FMO coefficients in a given MO. The qualitative outcome in terms of s, p, and d orbital participation in bonding remained unchanged, however, this criterion did not identify in all cases the most strongly bonding MOs. Certainly, a careful analysis of minimizing the need for an arbitrary decission as well as a more comprehensive analysis of choice dependence of MO s/p/d character would make the analysis more transparent but is behind the scope of the current study.

Table S6a: Lowest MOs with contribution of metal 6s orbital larger than 0.05 el., relative position of the particular orbital to HOMO, and absolute metal 6s-character in MO.

Compound	Lowest MO with s>0.05	Relative to HOMO	s-character
1	57	-2	0.23
2	58	-1	0.21
3	61	-2	0.22
4	62	-1	0.19
5	54	-5	0.26
6	52	-7	0.09
7	52	-7	0.24
8	56	-3	0.22
9	58	-5	0.26
10	56	-7	0.12
11	55	-6	0.20
12	54	-7	0.19

Table S6b: The lowest MO with 6p orbital contribution larger than 0.05 el., relative position of the observed orbital to HOMO, and amount of 6p-character in the MO.

Compound	Lowest MO with p>0.05	Relative to HOMO	p-character
1	62	+3	0.08
2	62	+3	0.06
3	67	+4	0.08
4	66	+3	0.05
5	59	0	0.05
6	66	+7	0.87
7	66	+7	0.86
8	59	0	0.05
9	60	-3	0.05
10	59	-4	0.05
11	61	0	0.06
12	60	-1	0.05

Table S7: NBO analysis of M–N1 and M–C2' bonds in compounds **1-12**. Atom contribution in %.

HA-LA bond	Atom	1	2	3	4	5	6	7	8	9	10	11	12
M–N1	N1	83.3	82.1	82.8	82.1	81.3	85.2	81.1	85.2	80.8	85.0	82.5	85.2
	M	16.7	17.9	17.2	17.9	18.7	14.8	18.9	14.8	19.2	15.0	17.6	14.8
M–C2'	C2'	65.2	68.0	64.7	65.8	67.4	63.8	62.3	67.3	66.4	61.1	65.2	58.6
	M	34.8	32.0	35.4	34.2	32.6	36.2	37.7	32.7	33.6	38.9	34.8	41.4

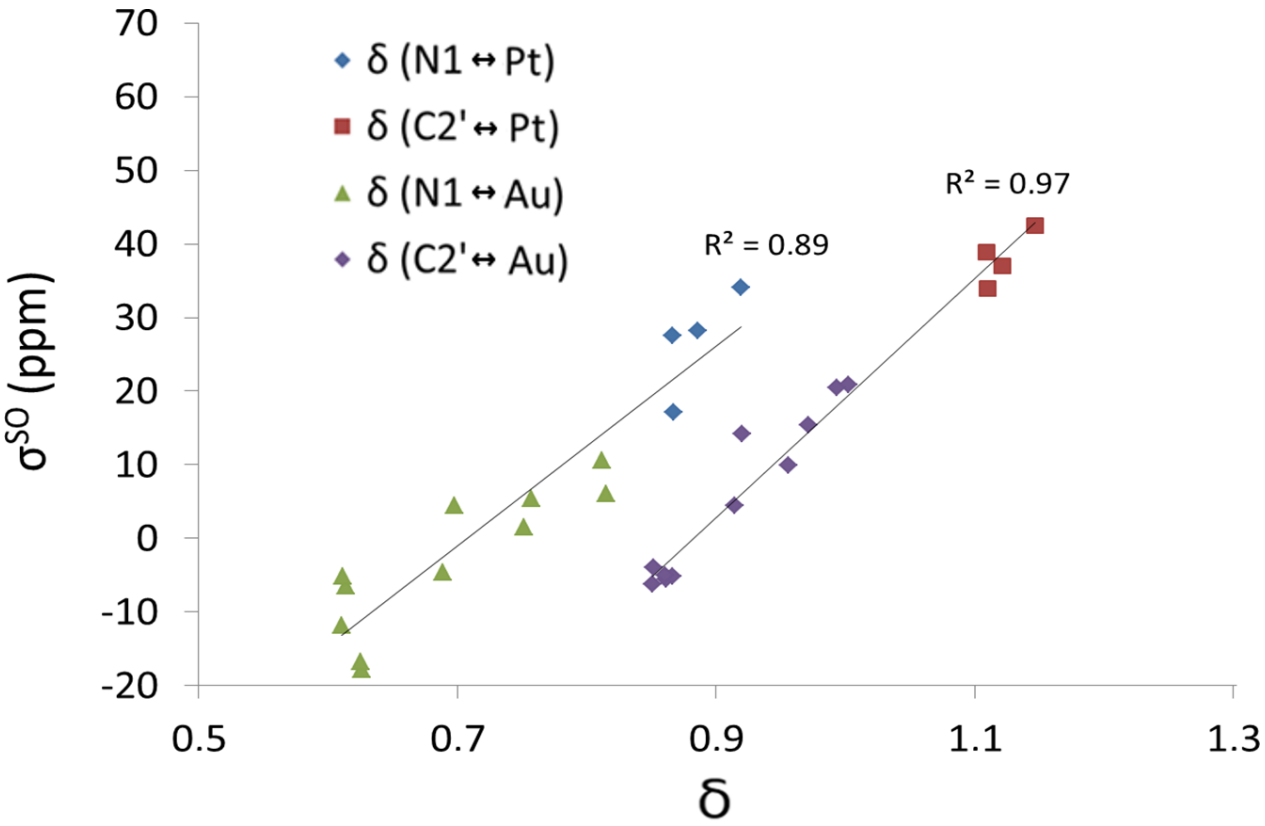

Figure S5. Correlation between the σ^{SO}(LA) and the delocalization index δ(M↔LA) for the M–LA pair of atoms. The series includes platinum (nitrogen – blue rhomb, carbon – red square) and gold (nitrogen – green triangle, carbon – violet rhomb) complexes.

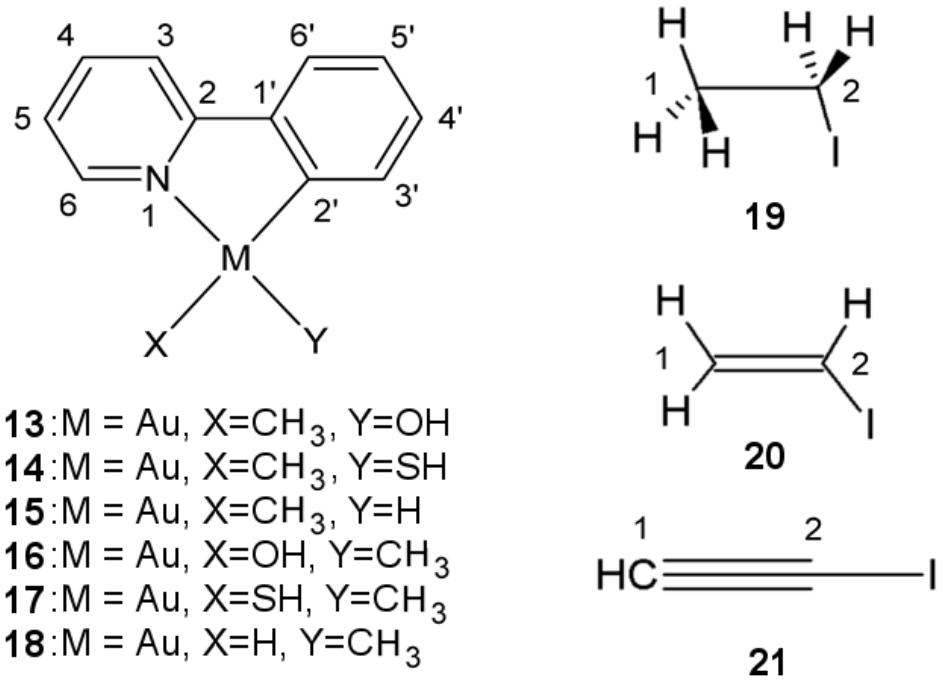

Figure S6. Structures of compounds **13-21** presented in the main text in **Figure 7**.

Table S8a: QTAIM electron delocalization indices and σ^{SO}(LA) for **1–18**. σ^{SO}(LA) in ppm.

Compound	δ (N1|M)	σ^{SO}(N1)	δ (C2'|M)	σ^{SO}(C2´)	δ (*trans* N1-M)	δ (*trans* C2'-M)
1	0.9192	34.1	1.1210	37.0	0.8003	0.5969
2	0.8857	28.2	1.1463	42.5	0.7786	0.6886
3	0.8674	17.2	1.1090	38.9	0.9936	0.6073
4	0.8659	27.5	1.1100	34.0	0.7859	0.8239
5	0.8115	10.6	0.8610	-5.5	0.8617	0.8628
6	0.6259	-17.8	1.0022	20.9	0.9618	0.7411
7	0.8149	6.0	0.9931	20.5	0.8672	0.7272
8	0.6139	-6.5	0.8664	-5.2	0.9614	0.8807
9	0.7516	1.5	0.8519	-4.0	1.0348	0.8602
10	0.6105	-11.8	0.9561	9.9	0.9517	0.8792
11	0.6977	4.4	0.8609	-5.0	1.0243	0.8593
12	0.6250	-16.7	0.9199	14.2	0.9459	0.8864
13	0.7572	5.4	0.8677	-3.1	1.0046	0.8617
14	0.6884	-4.6	0.8627	-0.6	1.1356	0.8541
15	0.6115	-5.2	0.8930	-5.7	0.9617	0.8945
16	0.6330	5.4	0.9714	15.4	0.9624	0.8661
17	0.6199	-7.8	0.9145	4.4	0.9541	0.9961
18	0.6396	-10.3	0.8505	-6.2	0.9733	0.9048

Table S8b: QTAIM electron delocalization indices and σ^{SO}(LA) for **19 - 21**. σ^{SO}(LA) in ppm.

Compound	δ (C1|I)	σ^{SO}(C1)
19	1.0969	27.0
20	1.1908	37.3
21	1.3120	56.7

[1] Malkin, V. G.; Malkina, O. L.; Salahub, D. R. *Chem. Phys. Lett.* **1996**, *261*, 335–345.

[2] (a) Mealli, C.; Proserpio, D. M. *J. Chem. Educ.* **1990**, *67*, 399. (b) Mealli, C.; Ienco, A.; Proserpio, D. M. *Book of Abstracts of the XXXIII ICCC*, Florence, Italy, 1998; Abstr. 510.

[3] Munzarová, M.; Hoffmann, R. *J. Am. Chem. Soc.* 2002, 124, 4787-4795.

[4] Eckert-Maksić, M. in *Theoretical Models of Chemical Bonding, Part 3*; Maksić, Z. B.; Ed., Springer, Berlin, 1991, pp 153-199.